

DESIGN AND CHARACTERIZATION OF A HYPERSPECTRAL CAMERA FOR LOW LIGHT IMAGING WITH EXAMPLE RESULTS FROM FIELD AND LABORATORY APPLICATIONS

J. Hernandez-Palacios^{a,*}, I. Baarstad^a, T. Løke^a, L. L. Randeberg^b, T. Skauli^c

^aNorsk Elektro Optikk AS, Solheimveien 62A, N-1471 Lørenskog, Norway –
(julio, baarstad, trond)@neo.no

^bDepartment of Electronics and Telecommunications, Norwegian University of Science and
Technology, N-7491 Trondheim, Norway – lise.randeberg@iet.ntnu.no

^cNorwegian Defence Research Establishment, P O Box 25, 2027 Kjeller, Norway –
Torbjorn.Skauli@ffi.no

KEY WORDS: Hyperspectral imaging, low-light imaging, photon noise, fluorescence, EMCCD.

ABSTRACT:

Hyperspectral imaging under low light level conditions has a potential use in a variety of applications including remote sensing and medical diagnostics. For most conventional hyperspectral sensors, however, performance is limited by the amount of photons available in the scene. In this work we describe the design and characterization of a hyperspectral camera for which sensitivity has been improved close to the photon-counting limit using an electron multiplying CCD array as light sensing element. The resulting hyperspectral camera is capable of operating in a wide range of illumination conditions with SNR values dependant on light intensity. Example results from field and laboratory measurements containing hyperspectral data from poorly illuminated scenes are given. The limitations of this approach and an interpretation of the data in terms of the photon noise associated with the signal are also discussed.

1. INTRODUCTION

Hyperspectral imaging is used for a broad range of applications in remote sensing and industry. It is also increasingly being used in other fields such as chemical research and medical diagnostics. Such versatility comes from its capability for recording and processing the spectral signatures of the materials being observed. However, this capability is highly dependent on the amount of light interacting with the material since incoming photons are separated into many spectral bands. A fundamental limitation arises when the number of photons is so low that relevant spectral contrasts are obscured by photon noise. Furthermore, in most hyperspectral

cameras the internal noise sources dominate over the signal in low light level conditions. There is however a number of applications where spectral imaging at such levels is of interest, e.g. low-light remote sensing and several fluorescence-based techniques ranging from standoff chemical imaging to fluorescence microscopy (Randeberg, L.L., 2006; Sinclair, M.B., 2006).

To enable the exploration of a range of potential applications, we have designed a low-light hyperspectral camera for the visible and near-infrared spectral range based on the HySpex VNIR-1600 design (NEO, 2009) and an electron-multiplying CCD (EMCCD) image sensor. Here, we describe the design and characterization of the camera and present illustrative results from preliminary tests. We

* julio@neo.no; phone: +47 67 97 47 00

also illustrate how knowledge of the photon noise level can be exploited in image analysis.

2. CAMERA DESIGN

2.1 Electron-multiplying CCD

The detector used is an iXon^{EM+} DU-897 back-illuminated EMCCD from Andor Technology PLC. It has 512×512 pixels with a pixel size of 16 μm, a full well capacity of 160 000 electrons and a peak quantum efficiency above 90%. The main feature of EMCCD sensors is the increased sensitivity to light by means of electron-multiplication gain (EMG). This consists of an additional register in the CCD architecture in which the signal from the pixels is progressively amplified (Denvir, D.J., 2003). Using the adequate EMG settings, the readout noise can be reduced to a negligible level at the expense of a moderate increase in signal noise in the multiplication process. The detector used here has a specified noise factor of $\sqrt{2}$. By cooling to 200 K, dark current is essentially suppressed. Thus, with the proper camera settings the dominant source is random photon noise even near the photon counting limit.

The nominal gain setting of the camera does not correspond directly to the EMG factor. To calibrate the EMG response, a constant signal from a uniform light field was used. The gain setting was varied from no gain up to a value for which the output signal was close to saturation. This process was repeated for two light levels in order to overcome the readout noise and cover a wider gain range. EMG values used throughout the text are the actual amount of gain in the multiplication register according to our calibration.

2.2 Camera optics

The optical design is a modified HySpex VNIR-1600 camera, a pushbroom-scanning imaging spectrograph shown schematically in Figure 1. The light from the scene is focused by an aspheric mirror onto a slit that defines

the instantaneous FOV. Behind the slit, a second aspheric mirror collimates the light onto a transmission grating for spectral dispersion in a perpendicular plane to the slit. An objective lens focuses the light onto a two-dimensional CCD detector array. A more detailed description can be found in (Norsk, 2009). With the Andor iXon detector, the linear field of view is 13 degrees over 512 spatial pixels, or 0.45 mrad per pixel. To accommodate the enclosure of a cooled EMCCD array, the distance from the grating to the objective lens has been increased, with only a slight sacrifice in image quality.

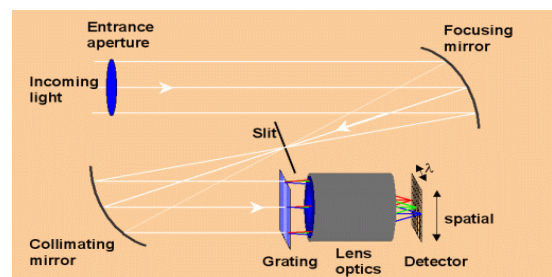


Figure 1. Schematic of the optical layout of the HySpex VNIR-1600 hyperspectral camera.

The camera software reads out a window of 100 pixel rows on the EMCCD array corresponding to the wavelength range 360 to 790 nm. The resulting spectral sampling interval is 4.3 nm. An order sorting filter mask is not fitted in the current version of the low-light camera due to a mechanical conflict with the EMCCD enclosure. Therefore, some spectral crosstalk may occur in the longwave part of the spectrum from second-order diffraction of light at shorter wavelengths. In the fluorescence tests described below, such crosstalk was eliminated by a 400 nm long-pass filter at the entrance aperture of the camera. In the remote sensing tests, no filter was used, to maximize light throughput.

3. RESULTS AND DISCUSSION

3.1 Night time target classification

The camera was mounted on a rotation stage to record ground-to-ground hyperspectral

images of two open semi-urban areas at night during the winter in the outskirts of Oslo, Norway. The dominating illumination contribution in the images comes from artificial sources (e.g. streetlights), directly and scattered by snow and other topographic features. The intensity of the overall light signal was measured using a luxmeter, averaging less than 0.2 lux during the recordings. As a comparison, 1.0 lux corresponds to the illumination conditions of a full moon night (Schubert, E. F., 2006).



Figure 2. Six colored jackets are used as targets during the test (a and b). A detail from the hyperspectral image highlighting the targets with its corresponding color is shown in (c). The spectrum from each jacket is shown in (d) according to their color.

The first scene is shown in Figure 2, at a distance of about 50 m from the camera. Figure 2 a) shows the scene in daylight before the actual measurements. Six jackets of different colors are used as targets. These are placed at different positions in front and between the trees as detailed in b). An RGB (600, 578 and 544 nm) image of the inset based on the hyperspectral image taken at night time is shown in Figure 2 c). Photon noise is evident as graininess in the image, but the system is clearly able to record usable data at this low light level. Sample spectra from the targets are shown in d). For this image, the camera was set at an integration time (IT) of 500 ms and EMG = 700.

As an illustration of the use of sensor noise estimates in image processing, consider the results shown in Figure 3. Here a simple Mahalanobis Distance classification algorithm has been used to try to separate targets, as well as the trees, from each other and from the snow background. The classifier is trained on small regions on each type of object within the same image. The classification result is shown in Figure 3 a). Generally, the five coloured jackets, as well as the trees, are separable from each other and from the snow. However the white jacket appears inseparable from the snow background.

It is not immediately clear whether the problem with the white jacket is due to a shortcoming of the simple algorithm used or whether it is an inherent limitation in the data. However, the photoelectron count gives useful insight into the noise level (Skauli, 2009) and allows us to analyze the separability of objects in terms of photon noise. The photoelectron count is a random variable with a Poissonian distribution, so that the variance is equal to the mean. Therefore, a good estimate of noise is obtained by calculating the number of photons corresponding to each DN value, and then taking the square root as an estimate of the standard deviation.

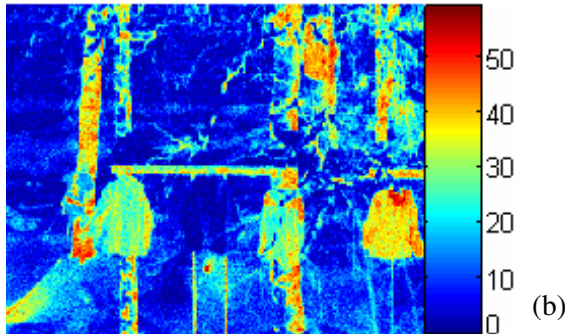
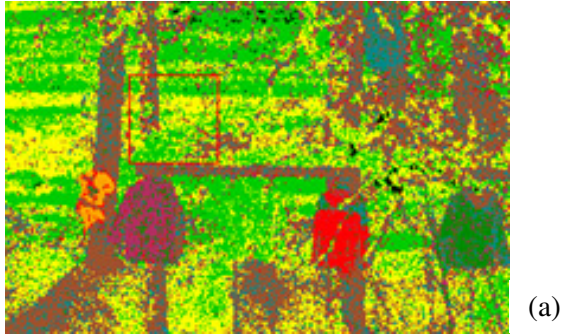


Figure 3. (a) The signal from the white target shows no contrast against the snow after the supervised classification algorithm. The plot in (b) shows the number of spectral bands in which the white target is separable from the rest of the image pixels.

A simple way to analyze the separability in terms of sensor noise, is to count the number of bands in which two spectra differ by more than the photon noise. Here we take the mean spectrum of the training pixels on the white jacket as a reference spectrum against which we compare all pixels in the image. For each pixel spectrum, we count the number of bands where the 1-sigma confidence intervals overlap, *ie* where the difference in photoelectron counts is larger than the sum of the estimated standard deviations of photoelectron count for the test pixel and reference spectrum. Thus the test is based on knowledge of sensor noise, rather than on variances estimated from the image.

The plot on Figure 3 b) shows, for each pixel, the number of bands in which the pixel signal is spectrally separable from the white target sample according to the criterion stated above. It is clear that there are generally very few spectral bands in which the snow is separable from the target. Hence it can be

concluded that photon noise is a sufficient explanation for the inseparability between the white jacket and snow.

This elementary analysis is of course a simplistic treatment of the data. Nonetheless it illustrates the potential usefulness of sensor-derived noise estimates, as well as of data formats that carry information about signal-dependent noise (Skauli, T. 2009).

3.2 Night scene with large dynamic range

The camera was also tested in a scene with high dynamic range, comprising bright light sources spatially close to deep-shadow area. See Figure 4. Images were recorded with multiple exposure times to capture the scene dynamics. Here we show results based on two images, one with integration time 100 ms and EMG=700 and another with integration time 10 ms and EMG=70. The figure shows the RGB (600, 548 and 458 nm) bands from the scene at night in the image with the longer exposure time. The signal on the sensor saturates close to the street lights in the scene. This can be seen in the spectrum plot for the bands around 600 nm. However, since the images are co-registered, saturated pixels can be straightforwardly replaced with data from the image recorded at the shorter integration time. Figure 5 shows the reconstructed spectrum based on the combined images. As a result the dynamic range of the image has also been enhanced, yielding a total dynamic in the image of approximately 4×10^5 or 112dB which is equivalent to having a 19-bit image.

The vertical streaks in Figure 4 are due to a combination of stray light and CCD smear. These effects are small relative to the total dynamic range of the combined image, but clearly visible in the data from the long exposure time. An interesting aspect of the high dynamic range is that it allows these sensor nonidealities to be characterized accurately, with the potential to compensate for most of the image degradation in a post-processing step.

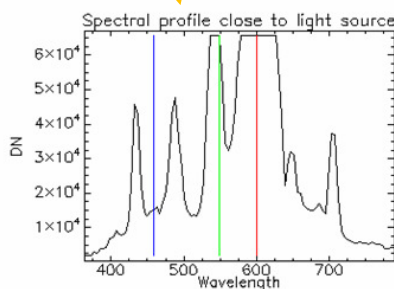


Figure 4. Strong illumination saturates the sensor in the spectral bands around 600 nm as the FOV approaches the source. The vertical stripes are due to stray light and CCD smear.

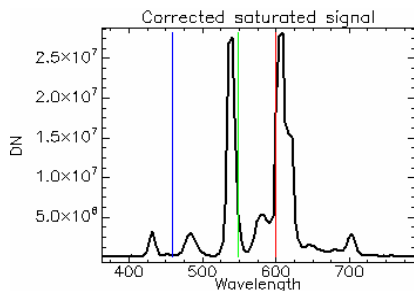


Figure 5. Spectrum of a saturated pixel after correction. The dynamic range of the image is also enhanced after correction.

3.3 Low light fluorescence measurements

The camera was also used to record hyperspectral images of fluorescent signals from organic tissue samples. For these measurements a diffused tripled Nd:YAG laser (355 nm, 7 mW/cm²) was used to excite natural fluorophores in the surface of ham samples. The samples were placed on a translation stage and scanned through the

camera field of view. The object distance was 30 cm. Different integration times ranging from 10 to 80 ms and EMG = 25 were used for these tests. Figure 6 show an RGB (600, 578 and 544 nm) image of the ham sample, and a plot of the spectra from different sectors on the sample.

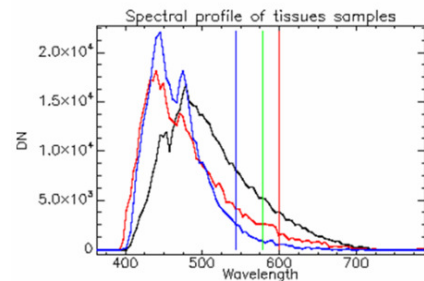
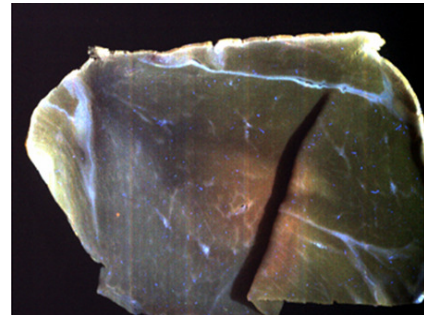


Figure 6. The natural fluorophores in a ham sample are excited using UV light. The profiles correspond to different fatty tissue constituents in the sample.

The capability to perform low light level measurements also enhances the applicability of this technology in fluorescence-based applications. A qualitative comparison of the results from the laboratory measurements show that power from the UV source can be reduced to at least 1/4 of the power used for similar experiments with a conventional HySpex VNIR-1600 camera. In principle, this allows to reduce the integration time and UV power further and still get high quality images using higher EMG values. These benefits are particularly promising for fluorescence-based medical diagnostics, where minimal exposure to UV light is aimed.

4. CONCLUSIONS

We have demonstrated hyperspectral imaging in various low light level conditions using an

EMCCD detector array in a HySpex imaging spectrometer. The example results show that multi-exposure images can capture scenes with wide dynamic range, with potential to correct for residual sensor artifacts. A fundamental limitation on the applicability of the camera is in general imposed by photon noise. The photon noise is signal-dependent, and it has been shown that sensor-derived noise estimates can be useful in analysis of hyperspectral images. Generally, low-light hyperspectral imaging has many potential applications, as illustrated by the examples given here.

REFERENCES

Denvir, D.J., 2003. Electron Multiplying CCDs. *Proc. SPIE*, Vol. 4877, pp. 55-68.

Norsk Elektro Optikk, 2009. HySpex Hyperspectral Cameras – An Overview. <http://www.neo.no/hispex/>

Randeberg, L.L., 2006. Hyperspectral imaging of bruised skin. *Proc. SPIE*, Vol. 6078, pp. 100-110.

Schubert, E. F., 2006. *Light-emitting diodes*. Cambridge University Press, pp. 278.

Sinclair, M.B., 2006. Hyperspectral confocal microscope. *Applied Optics*, Vol. 45, pp. 6283-6291.

Skauli, T., 2009. Sensor-informed representation of hyperspectral images. To be published in *Proc. SPIE*, Vol. 7334.

ACKNOWLEDGEMENTS

This work has been supported by the European Community's Marie Curie Research Training Networks Programme under contract MRTN-CT-2006-035927, Hyperspectral Imaging Network (HYPER-I-NET).